Planetary and Space Science 59 (2011) 1222–1230

Contents lists available at ScienceDirect

Planetary and Space Science

journal homepage: www.elsevier.com/locate/pss

Multilayer simulations for accurate geological interpretations of SHARAD radargrams

M.G. Spagnuolo [a,*], F. Grings [b], P. Perna [b], M. Franco [c], H. Karszenbaum [b], V.A. Ramos [a]

[a] Laboratorio de Tectónica Andina, Facultad de Ciencias Exactas y Naturales, Pab. 2, Ciudad Universitaria, Buenos Aires, Argentina
[b] Instituto de Astronomía y Física del Espacio (IAFE), Ciudad Universitaria, Buenos Aires, Argentina
[c] Universidad de Buenos Aires, Facultad de Ciencias Exactas y Naturales (FCEyN), Departamento de Física, Ciudad Universitaria, Pab. I, 1428 Buenos Aires, República Argentina

ARTICLE INFO

Article history:
Received 29 March 2010
Received in revised form
25 October 2010
Accepted 26 October 2010
Available online 3 November 2010

Keywords:
SHARAD
Mars
Simulation
Radargram
Subsurface mapping

ABSTRACT

SHARAD (SHAllow RADar) is a nadir-looking Synthetic Aperture Ground Penetrating Radar on board NASA's 2005 Mars Reconnaissance Orbiter. There are three main characteristics that define the performance of this instrument: ground penetration (due to the operational frequency, the observed echoes can be related to reflections from surface or subsurface), spaceborne operation (the first reflection does not necessarily correspond to the nadir reflection), and nadir looking SAR (there will always be left/right ambiguities). All this implies that there will be surface/subsurface range ambiguity and the geological interpretation of the radargrams cannot be straightforward. In order to avoid data misinterpretation, a simulator of SHARAD's expected response for a given observation geometry and topography is needed. Simulations can take into account all surface/subsurface reflections in order to identify common families of ambiguities and facilitate the interpretation. In this work we present SHARSIM (SHARAD Radargram SIMulator), a software tool designed to simulate SHARAD radargrams taking as inputs Mars surface information and hypothetical subsurface structure. Its performance is analyzed by investigating typical artifacts and by a direct comparison with real radargrams. We show that SHARSIM simulations can help to discern between artifacts and real subsurface features in order to make accurate geological interpretations.

1. Introduction

SHARAD (SHAllow RADar) is a nadir-looking Synthetic Aperture Ground Penetrating Radar on board NASA's 2005 Mars Reconnaissance Orbiter (Seu et al., 2007). SHARAD is capable of monitoring the first 2 km of Mars subsurface and therefore potentially discriminate layers of different materials in the Martian upper crust with an average vertical resolution of 15 m (dependent on material relative permittivity). The principal SHARAD objective is, as Seu et al. (2007) stated, is "to map, in selected locales, dielectric interfaces to at least several hundred meters depth in the Martian subsurface and to interpret these results in terms of the occurrence and distribution of expected materials, including competent rock, soil, water and ice". To this end, SHARAD is very well suited, since the relative permittivity of ice is different than the permittivity of rocks. A secondary, geologically related objective is to identify Mars subsurface dielectric interfaces and to interpret them in terms of geological processes at different environments.

Orbital radars are instruments capable of obtaining reflectivity maps from a planet surface at a given frequency and incidence angle. Reflectivity depends on both geometrical and dielectrical properties of the surface, and therefore carries information about surface structure and composition. A typical (side looking, not GPR) SAR can be considered an instrument capable of transforming reflectivity maps measured in the time delay/Doppler shift coordinates into range/azimuth coordinates. The algorithm responsible of this transformation is called SAR processor, and is a key step to obtain reliable reflectivity maps. There are several, well documented, SAR processing artifacts that degrade or even destroy the information content of some areas the reflectivity maps (Cumming and Frank, 2005).

SHARAD is different from a typical SAR in two main aspects: (I) it is not a side looking radar and (II) it is a ground penetrating radar (GPR). Point (I) implies that there always will be left/right range ambiguity (Quegan and Kingsley, 1999), and (II) implies that there always will be subsurface/superficial range ambiguity (Daniels, 2004). This is due to the fact that the received echo is the result of the combination of (1) nadir surface echoes, (2) nadir subsurface echoes, (3) off-nadir surface echoes and (4) off-nadir subsurface echoes, reaching the radar before and after nadir surface echoes. In principle, all these echoes cannot be discriminated because there is no one-way relation between time delay/Doppler values and target

* Corresponding author. Tel.: +54 1115616569 65.
E-mail addresses: mauro@gl.fcen.uba.ar (M.G. Spagnuolo), verderis@iafe.uba.ar (F. Grings).

0032-0633/$ - see front matter © 2010 Elsevier Ltd. All rights reserved.
doi:10.1016/j.pss.2010.10.013

coordinates. Although it is assumed that the radargrams carries stratigraphic information about Martian crust, they cannot be interpreted straightforward as geological subsurface sections due to the ambiguities mentioned before. Several approaches have been proposed to this end (Campbell, 2002; Biccari et al., 2001; Holt et al., 2006; Nouvel et al., 2004; Russo et al., 2008).

All of these radargram simulators are based on hypotheses about the Martian subsurface dielectric structure and geometry, Martian surface geometry, and wave-matter interaction. In order to develop a reliable reflectivity map of Mars subsurface (related to real dielectric discontinuities), it is important to identify the type of artifacts produced by the system. These artifacts will depend on specific observation geometries and landscapes, but also on the hypotheses governing the simulation experiment. To identify artifacts and to help in radargram interpretations, we developed SHARSIM, a coherent simulator of the SHARAD system that takes as input: (1) Martian surface topography and dielectrical properties, (2) SHARAD ancillary data (orbital and system), (3) subsurface layer structure and dielectrical properties and (4) scattering models.

This paper presents an analysis of expected SHARAD artifacts using SHARSIM simulations for different geometrical and dielectrical conditions of Mars surface/subsurface. The paper is organized as follows. In Section 2, we present the hypotheses related to Mars surface/subsurface geometry and dielectric properties, and expected scattering characteristics at SHARAD frequency. In Section 3, we show some basic SHARSIM simulations over different Mars landscapes. In Section 4, we compare SHARSIM simulations to some real SHARAD radargrams, in order to analyze the overall consistence and the specific discrepancies. Finally, in Section 5 we discuss the result of the analysis and propose some future improvement of SHARSIM and future radar simulation software.

2. Target model

2.1. Surface model

Our two main sources of knowledge about Martian topography: Mars Observer Laser Altimeter (MOLA) on board NASA's Mars Global Surveyor mission (Smith et al., 2003) and Mars Digital Elevation Models (DEMs) derived from HRSC (Neukum et al. 2004; Jaumann et al., 2007). These DEMs differ in spatial resolution (both horizontal and vertical) and coverage. MOLA grids have a resolution of $1/128^\circ$ both in longitude and in latitude, corresponding to a horizontal distance of $\sim$500 m at the equator. MOLA vertical accuracy depends strongly on Mars region, but can be evaluated of the order of $\sim$1 m (Smith et al., 2003). DEMs have a resolution of the order of 50 m both in longitude and in latitude and $\sim$10 m vertical resolution (Neukum et al., 2004; Jaumann et al., 2007). HIRISE Stereoscopic derived DEMs vary in resolution according to processing steps and image quality, but values of the order of centimeters on both horizontal and vertical resolution was published (Ivanov and Rossi, 2009). Since high resolution data exceed Sharad's wavelength (λ) by many orders of magnitude, we decided to work with MOLA grid and HRSC DEMs where available.

According to the scattering theory, the scattering behavior of a random surface is a function of the bidimensional surface profile z and dielectric and magnetic properties of the surface. For relatively rough surfaces, where $2\pi\sigma/\lambda \sim 1$, where σ is typical standard deviation of surface heights, the scattering can be modeled using the geometrical optics model (Kirchhoff model with stationary phase approximation, Fung, 1994). Conversely, if $2\pi\sigma/\lambda \sim 0.3$, the scattering can be modeled using the physical optics model (Kirchhoff model with scalar phase approximation, Fung, 1994). All the complex behaviors are related to the resonance range $\lambda/10 < z < 10\lambda$. This is important because Martian surface is expected to have spatial frequency components in all ranges, and there is no theoretical scattering model able to take as input a general surface profile and to estimate its scattering behavior. Therefore, a scattering model reflecting a compromise must be selected.

At medium resolution (profiles of the order of λ) DEM provides important *in situ* data, and at low resolution MOLA's provides global measure of the surface relief ($\sim 10\lambda$). Some authors have implicitly or explicitly assumed that, at MOLA resolution, Mars surface can be modeled as a random surface characterized by a single correlation length. Biccari et al. (2001) assumes a fractal surface, characterized by a Hurst exponent, an *rms* slope and an exponential correlation length. Using MOLA, Russo et al. (2008) found an *rms* height of the order of several meters, above the threshold defined by Rayleigh's criterion (Fung, 1994).

Our objective is to build a model able to reproduce the most common and expect artifacts of SHARAD. To this end, the high resolution information of stereoscopic DEM is of no use, since at this scale: (1) roughness is not expected to produce large changes in the phase of the backscattered wave and (2) no variations of the dielectrical properties are expected. Therefore, accepting as input mid-resolution DEMs from MOLA and from HRSC, we have information of Mars surface as a set of vertical points separated by DEM's resolution.

There are several ways to construct a surface from 3D grid. The most common involves the use of facets, in which a rough surface is approximated through a series of small planar facets. The expected scattering is then obtained as the coherent sum of scattering from individual facets. This model is suboptimal in terms of spatial continuity, but has the advantage of being related to a simple scattering model. Therefore, this is the model selected in this paper. The consequences of this choice in the scattering behavior are analyzed in the following section, but it is important to mention that SHARSIM software can take as input any scattering model.

2.2. Surface scattering model

The scattering problem of the Mars surface at microwave frequencies can be considered as follows. First, Mars surface is assumed to be a bidimensional surface with a characteristic length L. A plane wave illuminates the surface with an incident elevation angle θ_i and an azimuth angle ϕ_i. The instrument received power P_r from the surface and can be modeled using the radar equation:

$$P_r = \frac{P_t G_0^2 \lambda^2}{(4\pi)^3} \iint \frac{\sigma(\theta,\phi)}{R^4} dA \tag{1}$$

where P_t is the transmitted power, G_0 is antenna gain, $\sigma(\theta, \phi)$ the backscattering coefficient of the surface element and R the range from the instrument to the surface element. Since we are using facets to model the surface, the backscattering of the illuminated area of the surface will be approximated by the sum of the backscattering of all facets:

$$\sigma^0 = \frac{\lambda^2 A}{(4\pi)^3} \sum_{i \in facets} \frac{\sigma(\theta_i,\phi_i)}{R^4} \tag{2}$$

where A is the facet area. Therefore, our electromagnetic problem reduces to estimate the backscattering of a facet at every incidence geometry. If we approximate every facet by a flat rectangular plate, we can use the approximation developed by de Adana et al. (2003):

$$\sigma^0(\theta,\phi) = \frac{4\pi}{\lambda^2} \frac{\sin^4(ka\sin\theta\cos\phi)}{k^4 \sin^4\theta\cos^4\phi} \cos^2\theta \tag{3}$$

where a is the plate length. This approximation works very well for flat plates, even non-conducting ones when corrected using Fresnel coefficients. But there is still a second problem: this approximation is valid only for perfectly flat plates; therefore, the scattering will be

confined to a very narrow angular beamwidth. This has been found to be unrealistic in most studies about microwave scattering of planetary surfaces (Campbell, 2002; Johnson et al., 2007). We must therefore take into account that the facets cannot be considered flat plates, since they must have some internal (although unknown) structure. It is important to understand that a distribution of heights and blocks inside the facet will imply a difference in phase of the scattered signal of every point (Campbell, 2002). These phase differences create interference patterns in the radiated fields that cause the incident energy to be radiated in directions different to the incident one. In SHARSIM, Hagfor's model (Johnson et al., 2007) was implemented in order to include this subresolution interference pattern in the facet's model. This model is related to scattering process where mirror like facets pointed to the radar produce strong peaks at smaller angles. The facets should be much larger than the illuminated wavelength, a requisite that is satisfied for SHARAD ($\lambda = 12.5$ m, $\delta_{MOLA} = 500$ m, $\delta_{HRSC\ DEMs} = 50$ m). The model also assumes a Gaussian distribution of surface heights, a single scale exponential autocorrelation function of the surface profile and an approximation to derive the autocorrelation function at the origin (Johnson et al., 2007). The backscattering coefficient is then modeled as

$$\sigma^0 = \frac{\Gamma C}{2}\left[\cos^4\theta + C\sin^2\theta\right]^{-3/2} \quad (4)$$

where Γ is the Fresnel coefficient of the surface and C is a constant normally assumed to be the square root of the expected *rms* slope (10^{-1}–10^{-2} m; Biccari et al., 2001). Therefore, we estimate the backscattering of every facet using Eq. (4), taking as input the DEM derived geometric properties and dielectric parameters directly derived from hypotheses about the surface material composition derived from literature (Cereti et al., 2007; Carter et al., 2009). Furthermore, we consider that the dielectric properties remain constant for the considered swath. The selected values for the different materials considered are summarized in Table 1.

2.3. Subsurface model

Little is known about the Martian internal crust structure. One common assumption states that Martian crust is a stratified medium consistent of several quasi-horizontal layers of different materials. The composition and thickness of these layers is still a subject to debate, since different geomorphologic theories about Mars formation and evolution predicts different layered structures (Baker, 2001; Zuber, 2001). In order to test hypotheses about which geological structure will be observable in different geological settings, we include in the simulation the possibility to add layers at different depths in the form of DEMs below the surface, with different geometrical and dielectrical properties. We take the following general assumptions:

1. The layers have uniform dielectric properties. Therefore, scattering will only occurs at structure's interfaces (dielectrical boundaries) but not between them. Scattering will occur downwards and upwards.
2. A wave crossing a medium of thickness d will suffer a delay equal to

$$\delta = \frac{d}{2c\sqrt{\varepsilon}} \quad (5)$$

3. A wave crossing a medium of thickness d will suffer an attenuation that can be approximated as

$$\frac{|\bar{E}_x(d)|}{|\bar{E}_x(0)|} = e^{-d\sqrt{2}\omega\varepsilon''/c\sqrt{\varepsilon}} \quad (6)$$

where ε'' is the medium conductivity.

Two sources of uncertainties arise: Which is the geometrical structure of the dielectric boundaries and which are their dielectric properties? The dielectric properties of any material are related to

Table 1
Adopted dielectric properties of materials.

Material	Dielectric constant real part (ε')	Attenuation (α)	Notes
Lava flow	4.27	0.0033	**Type 4** (basaltic-andesite with 50–15% H_2O ice) from (Marinangeli et al., 2007)
Basalt	5.48	0.00077	**Type 7**: basalt with $<15\%$ H_2O ice from (Marinangeli et al., 2007)

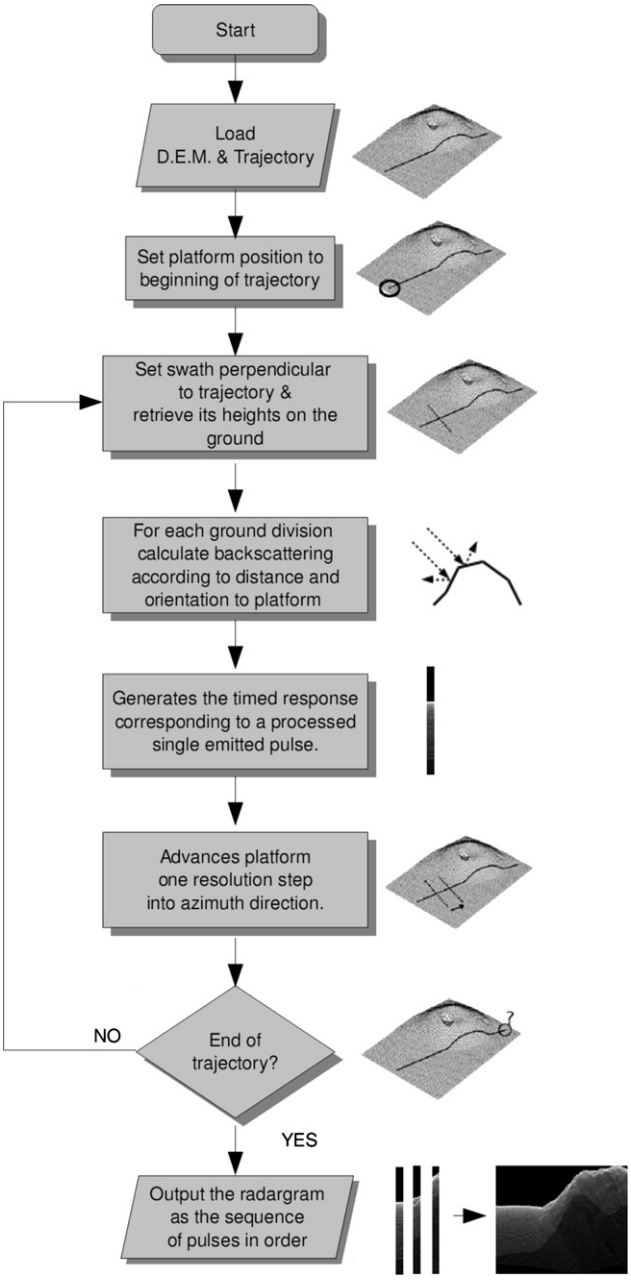

Fig. 1. SHARSIM flowchart.

their chemical structure. Therefore, if we assume a given layer composition we are defining its dielectrical properties. About boundaries geometry, no experimental information is available. But it is important to stress that SHARSIM allows the introduction of any given geometry.

3. Integration

The algorithm used to estimate the radargram for a given SHARAD observations geometry and Mars surface and subsurface is depicted in Fig. 1.

A few remarks are in order:

1. Platform trajectory is obtained from SHARAD ancillary information or can be synthesized in order to simulate hypothesized trajectories. SHARSIM simulates a swath of $\sim 1^{\circ}$.
2. Input DEM can be MOLA or HRSC.
3. In a real acquisition, SHARAD antenna footprint illuminates large regions of Mars surface. The reflections coming from before and after platform position is then compressed, using the Doppler information in the reflected pulse. The compression spatially localizes every pulse, effectively differentiating pulses coming from different azimuth positions (Cumming and Frank, 2005; Quegan and Kingsley, 1999). The simulation proposed in this paper assumes that azimuth compression is already done in an error free way. Therefore, the column of the radargram corresponding to every azimuth (along orbit) position is the coherent sum of the reflected pulses coming from surface or subsurface reflections. In future SHARSIM versions, this processing step will be simulated in order to include some specific artifacts related to azimuth compression.
4. The backscattering wave delay and attenuation of every subsurface facet is estimated using Eq. (4)–(6), and the backscattering of every surface facet is estimated using Eq. (4), using the values of Table 1 for the dielectric properties and DEM derived values for the geometric properties.
5. All these echoes are summed using (2) with their respective delays to obtain the simulated echo measured by SHARAD. Surface and subsurface propagation is done using raytracing techniques, estimating the backscattering for every facet in the corresponding surface/subsurface layer. A first order approach (no double or higher order bounces allowed) was selected due to the average low backscattering that characterizes the scattering at this wavelength. This is done for each spacecraft orbital position. The final product is SHARAD's simulated radargram.
6. This is a discrete simulation, since we are using a discrete DEM (MOLA or HRSC) and discrete intervals for range and azimuth positions. SHARAD also discretizes radar reflections in range using a constant time frame, and discretizes azimuth position using a constant PRF. However, actual Mars surface is continuous. This leads to a striping artifact, mostly seen in lower parts of the radargrams but actually corresponding to far off-nadir reflections.

4. Simulations

First, it is important to evaluate the differential quality in the radargrams simulated using DEMs from different resolutions. Therefore, we simulated the same Mars area using as input HRSC and MOLA DEMs. The result it is shown in Fig. 2.

As it can be seen from the figure, both simulated radargrams present the same artifacts related to geometrical features of Mars surface. In the selected area, the echoes coming from the craters near the path are easily observed in both simulations. However, in the zones near the smaller craters at the middle of platform track, the high resolution of HRSC DEM produces a radargram that reveals a complex reflection structure, unnoticed in the MOLA based simulation. In

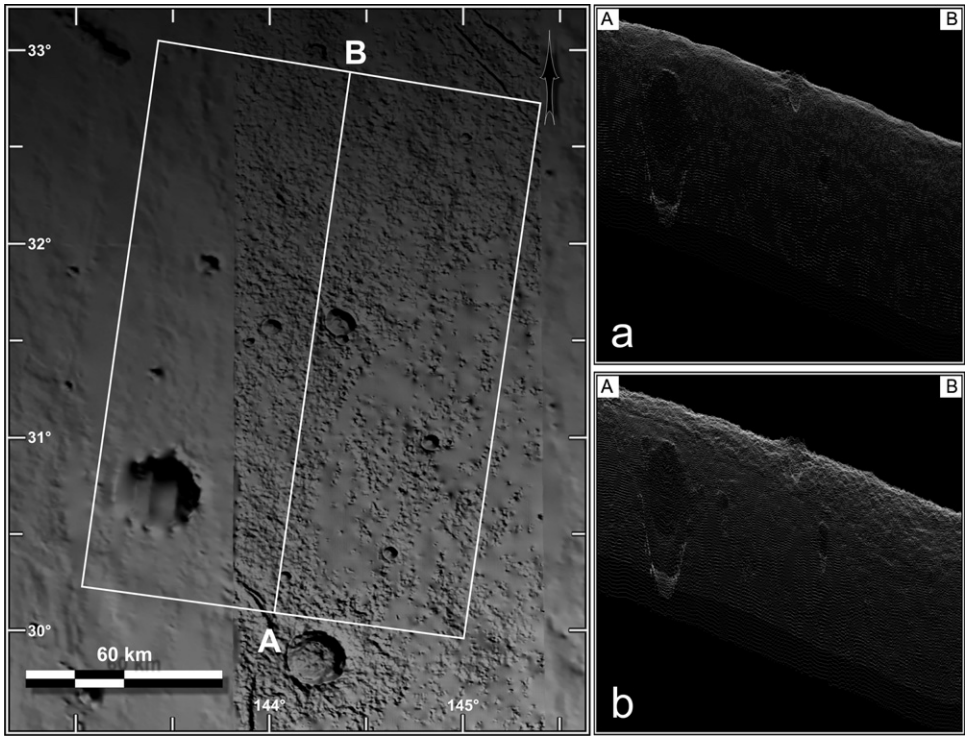

Fig. 2. To the left the figure shows a Mosaic of MOLA and HRSC DEMs used to compare simulated radargrams. Platform path and illuminated area is marked in white where simulation starting and ending points are marked as A and B, respectively. In the simulated radargrams (right, (a) MOLA only, (b) HRSC+MOLA). Although different from a quantitative point of view, the radargram simulated using the high resolution DEM do not present more or more complex artifacts but a better resolution due to more facets. (For interpretation of the references to color in this figure legend, the reader is referred to the web version of this article).

summary, with both DEMs we are able to identify off-nadir reflections (artifacts), which can be confused with subsurface reflections in a geological interpretation. Nevertheless, with high resolution DEMs, a more detailed simulation could be performed.

To evaluate SHARSIM performance, we will now evaluate simulated SHARAD radargrams over selected topographies, specifically chosen to maximize known artifacts. The first example is related to topographic artifacts. Since SHARAD has only one way to

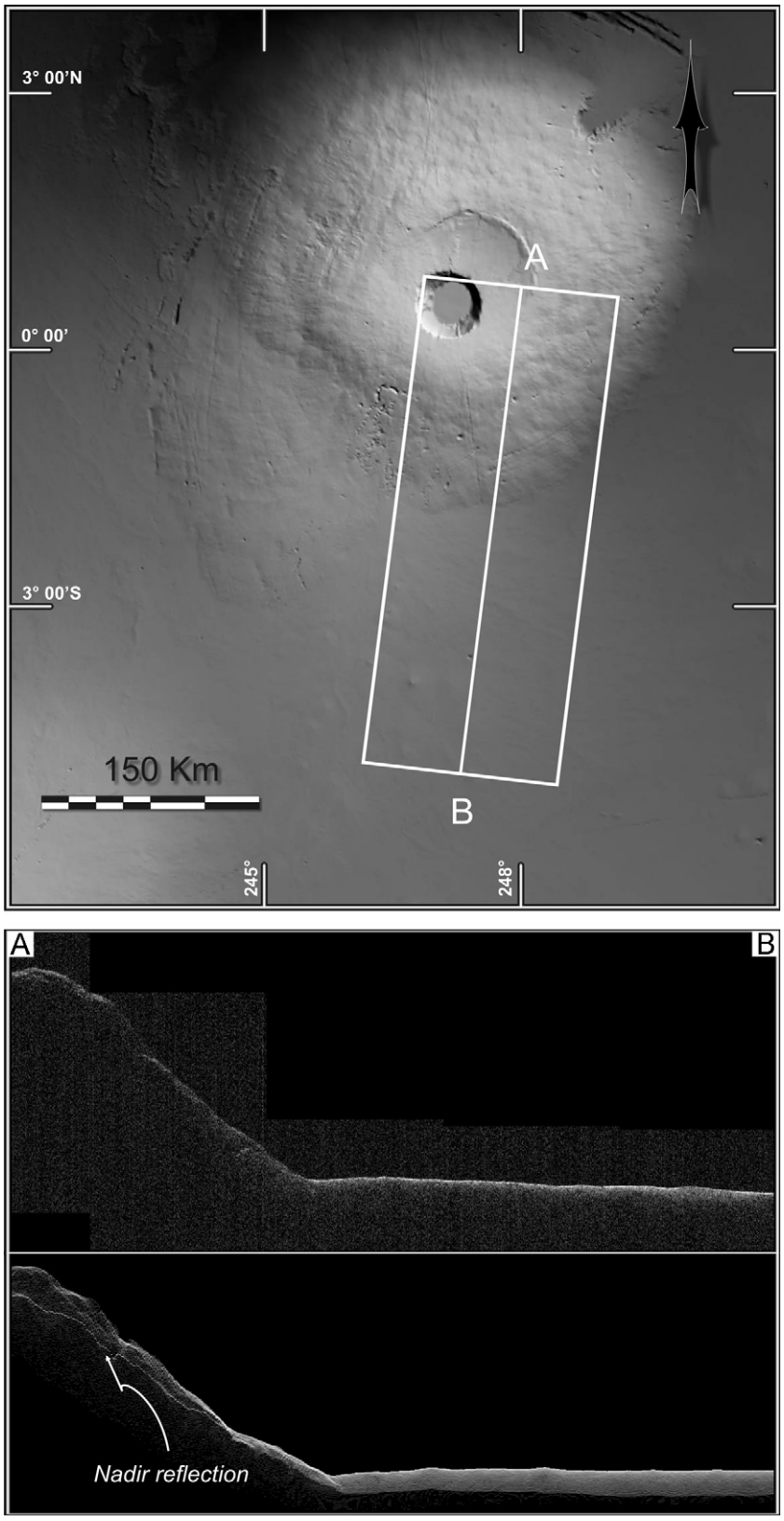

Fig. 3. Figure shows Pavonis mons MOLA DEM used to simulate the radargram (up). Platform path and illuminated area is marked in white (simulation start and end point is marked as A and B, respectively). In the simulated radargram (down) the nadir reflection is marked as dashed line. A series of reflection artifacts are easily identified.

differentiate pulses coming from across track direction (time delay), it cannot differentiate pulses coming from surface or subsurface. A typical artifact is observed when a large elevation is near but not crossing platform trajectory (Fig. 3). For some points of the elevation (a volcano in our case), the platform–surface distance is less that the platform–nadir distance. Therefore, the first pulses arriving are the ones corresponding to volcano's walls, and not from the surface. This will lead to a misinterpretation of the first radargram echo (actually coming from volcano's walls) as the nadir reflection. Moreover, the next radargram echoes (the ones actually coming from nadir) can be misread as subsurface reflections.

Furthermore, if the volcano walls happen to be perpendicular to the incoming EM wave, these reflections can be seen as intense as the nadir reflection. This will reinforce the wrong interpretation stated above and will assign a strong dielectrical change to the subsurface echo. Finally, from different parts of the volcano surface comes numerous echoes of varied intensity that arrives to the platform after the first echo. These echoes can also be misinterpreted as coming from subsurface structures. And it is important to remark that all these spurious reflections artifacts are produced in a simulation where there is no subsurface structure.

5. Comparison to real radargrams

In order to evaluate the full capabilities of SHARSIM, in Fig. 4 we compare a simulated radargram with a real one. The radargram corresponds to Biblis Tholus region, but the nadir track goes through a relatively flat area. As can be seen, there are two clear echoes in the real radargram, apparently coming from the subsurface. These echoes seem to be located at an average depth of ~400 m (assuming basalt materials (Biccari et al., 2001), see Eq. (5) and presents a strong reflection, similar in intensity to the surface echo. Theoretically, these kinds of reflections are typical of strong dielectrical discontinuities, such as atmosphere/basalt or basalt/pure ice (Cereti et al., 2007). This is reinforced by the fact that if these are subsurface echoes, they should suffer a non-negligible attenuation from the basalt soil (Biccari et al., 2001).

However, a direct comparison with the simulated radargram shows that these are artifacts, which may be produced by: off-nadir surface facet specular reflections related to topography, surface reflections related to an off-nadir very rough areas, or off-nadir reflections of surfaces with different dielectrical properties. Since there are no experimental evidences of a change in landcover related to a change in dielectrical or roughness properties, and there is a large topographic feature near, the best explanation for these observed artifacts is that they are reflections from Biblis Tholus and Ulyses Tholus lateral walls, which are not in platform nadir track but near it. Furthermore, more artifacts from both volcanoes are expected, some near the observed subsurface echoes and other arriving before the nadir reflections. However, these low power artifacts are not observed in the real radargram due to acquisition and processing limitations.

It is interesting to see that towards the tip of radargram track (B) and near the surface, there are also strong reflections that do not appear in the simulated radargram. This part of the track crosses over a relatively flat area dominated by lava flows, as can be seen in the Themis IR mosaic form (Fig. 5). These reflections do not seem to be related to topography artifacts, since they do not appear in the simulation.

In this kind of system, the width of a surface reflection is related to both the range resolution of the system and the nature of the target. The range resolution is related to chirp bandwidth, and for SHARAD, this value is around 15 m. The observed reflection is wider than the expected for a "point target" (a surface characterized by an ideal specular scattering pattern). Nevertheless, every surface presents a non-negligible superficial roughness, which leads to a wider scattering pattern. Therefore, every observed surface scattering in SHARAD is characterized by a wider than a pixel response. But in order to explain the observed reflection, whose width is not constant along track, two possible explanations arise: (1) the observation is the combination of two reflections from two separated layers not present on the whole

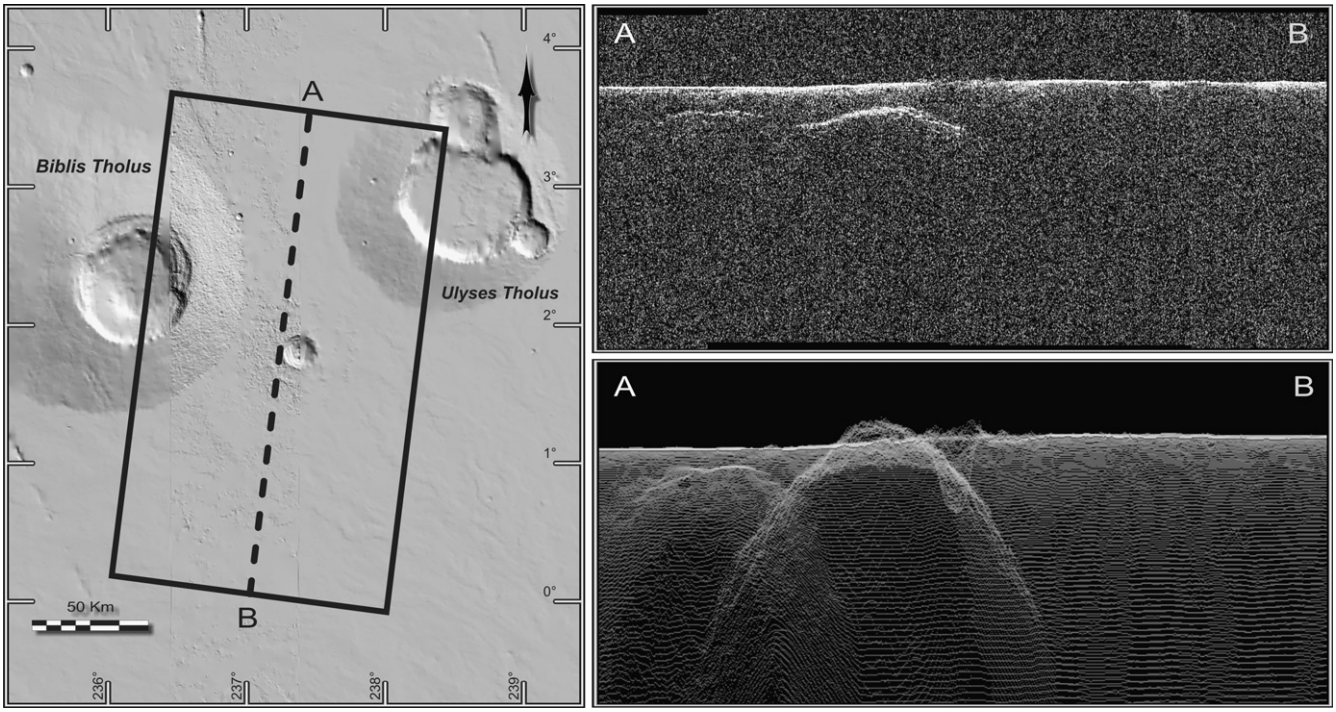

Fig. 4. Comparison between a real radargram and its simulation. To the left we show a location map made of MOLA and HRSC DEMs composition, with the path of radargram r_0193902_002_ss19_700_a along A–B dash-line and the simulated area marked in full line. To the right we compare the real radargram with the simulated one. (For interpretation of the references to color in this figure legend, the reader is referred to the web version of this article).

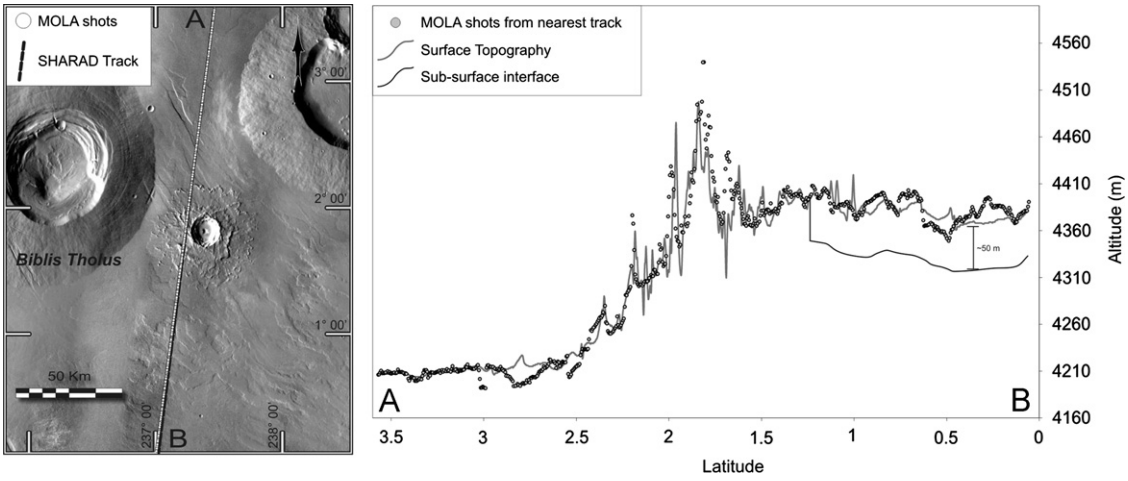

Fig. 5. This figure shows the track of the simulated radargram and MOLA shots over a TEMIS IR mosaic (left), and the topography profile along track (right). In grey is represented the surface topography used for simulation. Dots represent MOLA shots. The proposed subsurface topography for the simulation is shown in black.

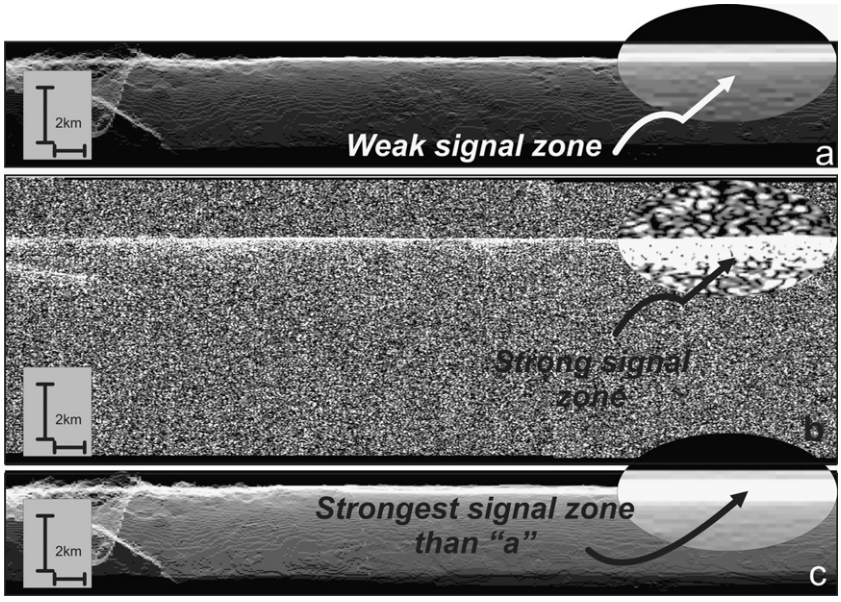

Fig. 6. Simulation of radargram r_0193902_002_ss19_700_a based on MOLA Mars topography of Biblis Tholus region with a hypothetical subsurface layer added (Fig. 5). (a) Simulation made using only the surface layer, (b) real radargram, (c) simulation made using the two dielectrical interfaces: one for vacuum/lava and another for lava/basalt (subsurface). The intense backscatter observed in the lava flows in region of the real radargram (b) is better simulated when a subsurface dielectric discontinuity is added (c).

track or (2) the observation arises from the changes in surface roughness along track. However, high resolution optical images do not show evidence of a significant change in surface roughness along track.

Therefore, we propose that these observed echoes come from a subsurface dielectrical discontinuity below the Mars surface. To test this hypothesis, we can use SHARSIM to simulate r_0193902_002_ss19_700_a radargram, but now considering both dielectrical discontinuities. However, we need as input parameters the layer depth, its geometrical structure and its permittivity. As an exercise, we will propose values for all these parameters, based on ancillary data or biographical information (see Table 1 and Carter et al., 2009).

To obtain a rough estimate of the lava flow thickness, we can use MOLA data. From MOLA shots, it can be seen that the lava flows are ~50 m thick tops (Fig. 5). Furthermore, we will suppose that there is basalt below the lava flow, so the adopted dielectric constant is the one corresponding to lava flow material for the region between the surface and the discontinuity and the one corresponding to basalt for the region below the discontinuity. Last, we will suppose that the layer and surface topography are similar. The proposed profile for the subsurface layer is shown in Fig. 5.

In order to test if our geological hypothesis is consistent with the observed radargram, we rerun the simulation of Fig. 4, but now including the proposed subsurface layer. The adopted dielectric constant was the one corresponding to lava flow material for the region between the surface and the discontinuity and the one corresponding to basalt for the region below the discontinuity. The result of the simulation is shown in Fig. 6.

It can be seen from the simulations that the addition of the subsurface layer increases radargram simulated backscatter of the lava flow region (B on Fig. 4). This agrees with SARAD observations better than the simulation without the subsurface structure (Fig. 6). However, it is important to remark that we are not claiming that there is a subsurface lava/basalt discontinuity in this region; we are just pointing out that the observed radargram is consistent with this hypothesis. There could be different geological configurations (related to different geometrical/dielectrical hypotheses) that lead to a radargram similar to the observed one. This is because there is

no one way relation between geological structure and SHARAD radargram. Therefore, in order to evaluate which subsurface geological set up it is more likely it is mandatory to use all the available information on the area, like optical images and radargrams at other frequencies.

6. Conclusion and future work

Although Mars exploration using remote sensing data is a relatively old discipline, only in the last 5 years there is enough information to test complex hypotheses about Mars geology using real data. Now, it is possible to test models about Mars condition and evolution using real information about soil hyperspectral reflectance Combe et al., 2008; Le Deit et al., 2008), topography (Smith et al., 2003; Neukum et al., 2004), subsurface dielectrical reflectivity in the microwave regime (Fois et al., 2007) and local gravity (Zuber et al., 2000).

Nevertheless, when using remote sensing data it is always important to distinguish between instrument measurement and geophysical information. This is particularly true for GPR instruments, for which a wide range of ambiguities are usually observed. There is information about Mars crust in SHARAD radargrams, but there is no one way relation between radargram scattering patterns and crust dielectric structures. In this paper, we have shown that there are predictable patterns of artifacts, mostly related to off-nadir surface scattering. Using SHARSIM, these artifacts are now predictable, since it is possible to simulate the expected SHARAD radargram from Mars topography information and ancillary data. Comparing these simulated radargrams with real ones, it is possible to identify artifacts from candidate subsurface reflections.

Moreover, it is possible to use SHARSIM as a predictive tool, given as input known data about Mars surface and data about hypothetical subsurface structures. Therefore, we can simulate the expected radargram corresponding to a complex medium (Mars surface and subsurface), which is a function of both geometrical and dielectrical hypotheses about the medium structure. These simulations are very important, since it is a rational way to test which geologically predicted subsurface structures for Mars are possible to identify using SHARAD and MARSIS.

For future work, we are including in the simulation more refined hypotheses about the scattering processes and the processing techniques. The first and most important is the simulation of the azimuth compression process, since there is a well-known set of artifacts related to this technique (Quegan and Kingsley, 1999). This is particularly relevant to forward looking GPR SAR systems, in which the spatiotemporal location of the impulse response function is a critical step in the compression scheme to correctly focus SAR echoes. Secondly, we plan to improve the scattering model by taking into account what is known about Mars small scale topography (of the order of centimeters) by using the integral equation method (Fung, 1994) to estimate the backscattering of DEM's facets. Early tests with this improved model predict a less extreme dependence of the backscattering coefficient with the incidence angle at large incidence angles, which is consistent with the observations. To this end high resolution topographies with submeter resolutions would be useful.

Acknowledgment

We want to thank CONICET for the financial support, Ph.D. J.C. Jacobo Berlles for their insight in radar processing, Ph.D. R. Orosei and Ph.D. A. Rossi for the support and COSPAR for the funding to attend to Mars Mapping workshop and R. Quenedi for the English review.

References

Baker, V.R., 2001. Water and the Martian landscape. Nature 412, 228–236. doi:10.1038/35084172.

Biccari, D., Picardi, G., Seu, R., Melacci, P.T., 2001. Mars surface models and subsurface detection performance in MARSIS. In: Proceedings of the Geoscience and Remote Sensing Symposium, 2001. IGARSS '01. IEEE 2001, vol. 6, pp. 2560–2562.

Campbell, B.A., 2002. Radar Remote Sensing of Planetary Surfaces. Cambridge University Press, Cambridge, pp. 342.

Carter, L.M., Campbell, B.A., Holt, J.W., Phillips, R.J., Putzig, N.E., Mattei, S., Seu, R., Okubo, C.H., Egan, A.F., 2009. Dielectric properties of lava flows west of Ascraeus Mons, Mars. Geophys. Res. Lett. 36, L23204. doi:10.1029/2009GL041234.

Cereti, A., Vannaroni, G., Del Vento, D., Pettinelli, E., 2007. Electromagnetic measurements on Martian soil analogs: Implications for MARSIS and SHARAD radars in detecting subsoil water. Planet. Space Sci. 55 (1–2), 193–202. doi:10.1016/j.pss.2006.06.002.

Combe, J.P., Le Mouelic, S., Sotin, C., Gendrin, A., Mustard, J.F., Le Deit, L., Launeau, P., Bibringd, J.P., Gondetd, B., Langevind, Y., Pinete, P., the OMEGA Science team, 2008. Analysis of OMEGA/Mars express data hyperspectral data using a multiple-end member linear spectral unmixing model (MELSUM): methodology and first results. Planet. Space Sci. 56 (7), 951–975.

Cumming, I.G., Frank, H.W., 2005. Digital Processing of Synthetic Aperture Radar Data: Algorithms and Implementation. Hardcover. Artech House, pp. 630, ISBN:101580530583.

Daniels, D.J. (Ed.), 2004. Knoval second ed. Institution of Engineering and Technology.

de Adana, F.S., Nieves, S., Garcia, E., Gonzalez, I., Gutierrez, O., Catedra, M.F., 2003. Calculation of the RCS from the double reflection between planar facets and curved surfaces. IEEE Trans. Antennas Propag. 51 (9), 2509–2512.

Fois, F., Mecozzi, R., Iorio, M., Calabrese, D., Bombaci, O., Catallo, C., Croce, A., Croci, R., Guelfi, M., Zampolini, E., Ravasi, D., Molteni, M., Ruggeri, P., Ranieri, A., Ottavianelli, M., Flamini, E., Picardi, G., Seu, R., Biccari, D., Orosei, R., Cartacci, M., Cicchetti, A., Masdea, A., Giacomoni, E., Cutigni, M., Provenziani, M., Fuga, O., Alberti, G., Mattei, S., Papa, C., Marras, P., Tattarletti, B., Vicari, D., Bonaventura, F., Paterno, T., Di Placido, A., Morlupi, A., 2007. Comparison between MARSIS & SHARAD results. In: Proceedings of Geoscience and Remote Sensing Symposium, 2007. IGARSS 2007, IEEE 2134–2139 (doi: 10.1109/IGARSS.2007.4423256).

Fung, A.K., 1994. Microwave Scattering and Emission Models and Their Applications. Artech House, London ISBN:0-89006-523-3.

Holt, J.W., Peters, M.E., Kempf, S.D., Morse, D.L., Blankenship, D.D., 2006. Echo source discrimination in single pass airborne radar sounding data from the Dry Valleys, Antarctica: implications for orbital sounding of Mars. J. Geophys. Res. 111, E06S24. doi:10.1029/2005JE002525.

Ivanov, A., Rossi, A.P., 2009. Investigation of small scale roughness properties of Martian terrains using Mars reconnaissance orbiter data. Geophysical Research Abstracts, vol. 11, #EGU2009-9426, Vienna.

Jaumann, R., Neukum, G., Behnke, T., Duxburry, T.C., Eichentopf, K., Van Gasselt, S., Giese, B., Gwinner, K., Hauber, E., Hoffmann, H., Hoffmeister, A., Köhler, U., Matz, K.D., McCord, T.B., Mertens, V., Oberst, J., Pischel, R., Reib, D., Ress, E., Roatsch, T., Saiger, P., Scholten, F., Schwarz, G., Stephan, K., Wählisch, M., the HRSC Co-Investigator Team, 2007. The high resolution stereo camera (HRSC) experiment on mars express: instrument aspects and experiment conduct from interplanetary cruise through nominal mission. Planet. Space Sci. 55, 928–952.

Johnson, J.T., Warnick, K.F., Peng, Xu, 2007. On the geometrical optics (Hagfors' law) and physical optics approximations for scattering from exponentially correlated surfaces. IEEE Trans. Geosci. Remote Sensing 45 (8), 2619–2629.

Le Deit, L., Le Mouélic, S., Bourgeois, O., Combe, J.P, Mège, D., Sotin, C., Gendrin, A., Hauber, E., Mangold, N., Bibring, J.P., 2008. Ferric oxides in East Candor Chasma, Valles Marineris (Mars) inferred from analysis of OMEGA/Mars express data: identification and geological interpretation. J. Geophys. Res. 113, E07001. doi:10.1029/2007JE002950.

Marinangeli, L., Pettinelli, E., Vannaroni, G., Cereti, A., Rossi, A.P., Baliva, A., Biccari, D., Seu, R. 2007. Inferring the dielectric properties of the surface of mars from martian missions and analogues samples. Lunar and Planetary Science XXXVIII, # 1619.

Neukum, G., Jaumann, R., the HRSC Co-investigator and Experiment Team, 2004. The high resolution stereo camera of mars express. In: Wilson, A. (Ed.), Mars Express: The Scientific Payload, 2004. ESA, Noordwijk, The Netherlands, pp. 17–35.

Nouvel, J.F., Herique, A., Kofman, W., Safaeinili, A., 2004. Radar signal simulation: surface modeling with the facet method. Radio Sci. 39, 1013.

Quegan, S., Kingsley, S., 1999. Understanding Radar Systems. SciTech Publishing Inc. ISBN-10:1891121057.

Russo, F., Cutigni, M., Orosei, R., Taddei, C., Seu, R., Biccari, D., Giacomoni, E., Fuga, O., Flamini, E., 2008. An incoherent simulator for the SHARAD experiment. In: Proceedings of the Radar Conference, RADAR '08. IEEE 2008, 26–30 May, pp. 1–4.

Seu, R., Phillips, R.J., Biccari, D., Orosei, R., Masdea, A., Picardi, G., Safaeinili, A., Campbell, B.A., Plaut, J.J., Marinangeli, L., Smrekar, S.E., Nunes, D.C., 2007. SHARAD sounding radar on the Mars Reconnaissance Orbiter. J. Geophys. Res. 112, E05S05.

Smith, D.E., Zuber, M.T., Frey, H.V., Garvin, J.B., Head, J.W., Muhleman, D.O., Pettengill, G.H., Phillips, R.J., Solomon, S.C., Zwally, H.J., Banerdt, W.B., Duxbury, M.T.C., Golombek, M.P., Lemoine, F.G., Neumann, G.A., Rowlands, D.D., Aharonson, O., Ford,

P.G., Ivanov, A.B., Johnson, C.L., McGovern, P.J., Abshire, J.B., Afzal, R.S., Guinness, E. A, A, Sun, X., 2003. Mars orbiter laser altimeter: experiment summary after the first year of global mapping of Mars. J. Geophys. Res. 106 (E10), 23689–23722 2001S. Slavney. Mars Global Surveyor Laser Altimeter Mission Experiment Gridded Data Record, MGS-M-MOLA-5-MEGDR-L3-V1.0, NASA Planetary Data System. URL: 〈http://ieeexplore.ieee.org/stamp/stamp.jsp?arnumber=4720761&isnumber=4720717〉.

Zuber, M.T., 2001. The crust and mantle of Mars. Nature 412, 220–227. doi:10.1038/35084163.

Zuber, M.T., Solomon, S.C., Phillips, R.J., Smith, D.E., Tyler, G.L., Aharonson, O., Balmino, G., Banerdt, W.B., Head, J.W., Lemoine, F.G., McGovern, P.J., Neumann, G.A., Rowlands, D.D., Zhong, S., 2000. Internal structure and early thermal evolution of Mars from Mars global surveyor topography and gravity. Science 287 (5459), 1788–1793.